Modeling and Simulation of Fractional Order PI Control Limiters for Power Systems ⋆

Mohammed Ahsan Adib Murad, Georgios Tzounas, Federico Milano

School of Electrical and Electronic Engineering,
University College Dublin, Ireland
{*mohammed.murad, georgios.tzounas*}*@ucdconnect.ie,*
federico.milano@ucd.ie

Abstract: The paper focuses on the modeling and simulation of Fractional Order PI (FOPI) control limiters for power system applications. One windup limiter and three anti-windup limiter models, namely back calculation; automatic reset; and conditional integrator method, are considered and compared. A numerical convergence issue that emerges in models that include FOPIs with the conditional integrator method is duly described. In the case study, the proposed FOPI models are utilized for voltage regulation through a static synchronous compensator. The limiter models are compared by carrying time domain simulations on the IEEE 14-bus benchmark system.

Keywords: Fractional Order PI (FOPI) control, anti-windup, power systems, transient stability.

1. INTRODUCTION

1.1 Motivation

In recent years, fractional calculus-based controllers have gained increasing attention in the power system community, mostly because of their robust performance for a wide range of operating conditions and parameter variations. However, the effect of control saturation on the dynamic behavior of Fractional Order (FO) controllers for power system applications has not been considered at all. This paper discusses modeling and simulation of windup and anti-windup limiters of the FO version of the classical PI controller (FOPI) for power systems.

1.2 Literature Review

The Proportional-Integral-Derivative (PID) control strategy is ubiquitous in many engineering applications due to its simple structure, easy tuning and overall good dynamic performance. In power systems, the PI is the most common configuration, as the derivative term can deteriorate the dynamic performance under the presence of noise and large disturbances (Åström et al., 2006).

The FOPI is an extension of the PI which stems from the theory of fractional calculus. Fractional calculus studies the differentiation and integration operations for non-integer (fractional) orders. The potential of employing fractional calculus for the purpose of control was first shown in the definition of Bode's ideal transfer function (Bode, 1945), while the frequency domain properties of FO controllers were systematically exploited first in (Oustaloup, 1991). To date, the FO version of the PID (FOPID) (Podlubny, 1999b), has been the most popular FO controller.

The utilization of FO controllers in power systems has been recently proposed for different applications, including voltage (Zamani et al., 2009; Shah et al., 2018), frequency (Debbarma et al., 2014; Pan and Das, 2015) and damping (Chaib et al., 2017; Abdulkhader et al., 2019) control schemes. The implementation of these controllers is done by means of approximating the fractional dynamics with rational order transfer functions (Vinagre et al., 2000). In this paper, fractional dynamics are approximated by the widely used Oustaloup's Recursive Approximation (ORA) method (Oustaloup et al., 2000).

The high significance of considering control limits is widely recognized in power systems. In particular, control limits play a crucial role when large disturbances are of interest, as it happens, e.g. in dynamic security assessment. Regarding PI controllers, the integrator windup phenomenon is known to severely limit the control performance (Åström et al., 2006). Consequently, there exists a handful of references on PI anti-windup (AW) methods and their impact on dynamic systems response (Glattfelder and Schaufelberger, 2012; Murad and Milano, 2019). Similar techniques are also proposed for FOPIs (Padula et al., 2012; Pandey et al., 2017). However, a systematic study of the impact and numerical issues of those classical methods on FOPIs for power system applications has not been given thus far. This paper fills this gap.

1.3 Contributions

The contributions of the paper are as follows.

⋆ This work is supported by the Science Foundation Ireland, by funding Mohammed Ahsan Adib Murad, Georgios Tzounas, and Federico Milano, under Investigator Programme Grant No. SFI/15/IA/3074.

- A discussion on the modeling of windup and AW limiters of FOPI controllers for power system applications.
- An in depth explanation of a numerical convergence issue during the time domain simulation with inclusion of the conditional integrator AW method.
- A comparison of the impact of FOPI limiter models on the AC voltage regulation of power systems through a Voltage Sourced Converter (VSC)-based Static Synchronous Compensator (STATCOM).

1.4 Organization

The remainder of the paper is organized as follows. Section 2 provides a background on the theory of fractional calculus for control applications. Section 3 presents the considered FOPI control models. The case study is discussed in Section 4, based on the IEEE 14-bus system. Conclusions and future work directions are drawn in Section 5.

2. THEORY OF FRACTIONAL ORDER CONTROL

2.1 Fractional Calculus

Fractional calculus provides the extension of differentials and integrals for non-integer number orders. There exist different formulations of fractional calculus. The most important ones are arguably the Riemann–Liouville (R-L); the Grünwald–Letnikov (G-L); and the Caputo definition. Each definition may be more or less suitable depending on the application.

For the purpose of the design of fractional controllers, the Caputo definition is the most appropriate. Consider a function $\phi : [0, \infty) \to \mathbb{R}$. In its derivative form, Caputo definition for the fractional derivative ϕ of order $\gamma \in \mathbb{R}^+$ reads (Monje et al., 2010):

$$\phi^{(\gamma)}(t) = \frac{1}{\Gamma(\mu - \gamma)} \int_0^t \frac{\phi^{(\mu)}(\tau)}{(t-\tau)^{\gamma-\mu+1}} d\tau \ . \tag{1}$$

where γ, $\mu - 1 < \gamma < \mu$, $\mu \in \mathbb{N}$, denotes the fractional order; $\Gamma(\cdot)$ is the Gamma function; and $\phi^{(\gamma)}(t) = d^\gamma \phi / dt^\gamma$. Unlike the R-L and G-L definitions, the initial conditions of (1) are of integer order. This property is of great importance, since for physical variables, only integer order initial conditions are known.

2.2 Fractional Order PID Control Strategy

The most popular FO control strategy is the FOPID (Podlubny, 1999a). The FOPID controller is an extension of the classical PID, and is characterized by five parameters: three gains, namely proportional, integral, and derivative; and two fractional orders, namely integral and derivative.

Employing a FOPID extends the four control points of the PID strategy to the plane defined by the orders α and β (Monje et al., 2010). This is illustrated in Fig. 1.

2.3 Approximation of Fractional Dynamics

Modeling of fractional dynamics is typically done by employing rational transfer functions that approximate the fractional derivatives and integrals. In this paper,

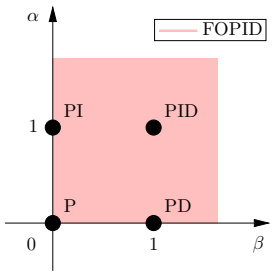

Fig. 1. PID vs FOPID: From point to plane.

fractional dynamics are approximated by the commonly employed ORA technique. Let $[\omega_b, \omega_h]$ be the frequency range for which the approximation is designed and N the dynamic order of the approximation. Then, the ORA of s^γ is defined as follows (Monje et al., 2010):

$$s^\gamma \approx \omega_h^\gamma \prod_{k=1}^{N} \frac{s + \omega'_k}{s + \omega_k} \ , \tag{2}$$

where

$$\begin{aligned} \omega'_k &= \omega_b \omega_v^{(2k-1-\gamma)/N} \ , \\ \omega_k &= \omega_b \omega_v^{(2k-1+\gamma)/N} \ , \\ \omega_v &= \sqrt{\omega_h / \omega_b} \ . \end{aligned} \tag{3}$$

The parameters in (3) are derived from a set of recursive equations (Oustaloup et al., 2000). The block diagram of the ORA is shown in Fig. 2.

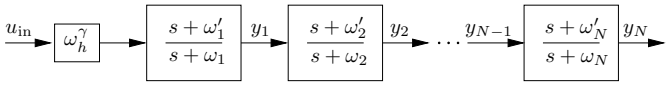

Fig. 2. Oustaloup's Recursive Approximation (ORA).

The accuracy of (2) deteriorates if high fractional orders, i.e. $|\gamma| > 1$ are to be used. In this case, the implementation consists in the product of an integer order block and a fractional order block, as follows:

$$s^\gamma = s^n s^{\gamma - n}, \ n \in \mathbb{Z}, \ (\gamma - n) \in [0, 1] \ . \tag{4}$$

Figure 2 shows that each block of the ORA is a lead-lag filter. In time domain, the ORA dynamic model can be described by a set of differential-algebraic equations, as follows (Baranowski et al., 2015):

$$\begin{aligned} \chi'_1 &= a_1 \chi_1 + b_1 \omega_h^\gamma u_{\text{in}} \\ 0 &= y_1 - \chi_1 - \omega_h^\gamma u_{\text{in}} \\ \chi'_2 &= a_2 \chi_2 + b_2 (\chi_1 + \omega_h^\gamma u_{\text{in}}) \\ 0 &= y_2 - \chi_2 - \chi_1 - \omega_h^\gamma u_{\text{in}} \\ &\vdots \\ \chi'_N &= a_N \chi_N + b_N (\sum_{k=1}^{N-1} \chi_k + \omega_h^\gamma u_{\text{in}}) \\ 0 &= y_N - \sum_{k=1}^{N} \chi_k - \omega_h^\gamma u_{\text{in}} \ . \end{aligned}$$

where $a_k = -\omega_k$, $b_k = \omega'_k - \omega_k$. Using matrix notation, we finally have:

$$\begin{aligned} \boldsymbol{\chi}' &= \boldsymbol{A}\boldsymbol{\chi} + \boldsymbol{B} u_{\text{in}} \\ 0 &= y_N - \boldsymbol{C}\boldsymbol{\chi} - \omega_h^\gamma u_{\text{in}} \ , \end{aligned} \tag{5}$$

where $\boldsymbol{\chi} = [\chi_1 \;\; \chi_2 \cdots \;\; \chi_N]^T$; and

$$\boldsymbol{A} = \begin{bmatrix} a_1 & 0 & 0 & \cdots & 0 \\ b_2 & a_2 & 0 & \cdots & 0 \\ b_3 & b_3 & a_3 & \cdots & 0 \\ \vdots & \vdots & \vdots & \ddots & \vdots \\ b_N & b_N & \cdots & b_N & a_N \end{bmatrix} \;, \; \boldsymbol{B} = \begin{bmatrix} \omega_h^\gamma b_1 \\ \omega_h^\gamma b_2 \\ \omega_h^\gamma b_3 \\ \vdots \\ \omega_h^\gamma b_N \end{bmatrix} \;,$$

$$\boldsymbol{C} = [1 \;\; 1 \cdots 1 \;\; 1] \;.$$

$\boldsymbol{A}$, $\boldsymbol{B}$, $\boldsymbol{C}$, have dimensions $N \times N$, $N \times 1$ and $1 \times N$, respectively.

3. FRACTIONAL ORDER PI SCHEMES

This section presents the FOPI schemes considered in this study. These include an unconstrained FOPI (FOPI0); a FOPI with windup limiter (FOPI1); a FOPI with a back calculation AW limiter (FOPI2); a FOPI with an automatic reset AW limiter (FOPI3); and a FOPI with a conditional AW model (FOPI4). The block diagrams of all five FOPI control schemes are shown in Fig. 3.

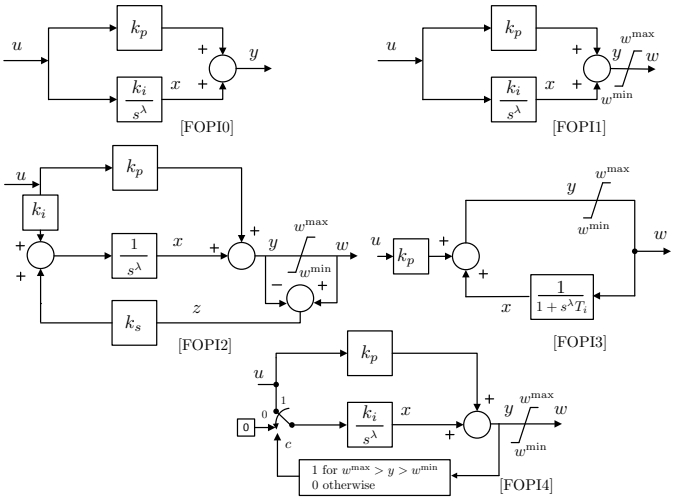

Fig. 3. Examined FOPI controller models: (FOPI0) without limits; (FOPI1) with windup limiter; (FOPI2) with back calculation AW limiter; (FOPI3) with automatic reset AW limiter; (FOPI4) with conditional AW limiter.

It is relevant to note here is that there exist several other AW schemes that one may consider. However, the considered models cover the most common configurations (Åström et al., 2006).

3.1 Unconstrained Model

Without considering any limits, the FOPI controller can be described as follows:

$$\begin{aligned} x^{(\gamma)} &= k_i u \\ y &= k_p u + x \;, \end{aligned} \tag{6}$$

where k_p, k_i are the proportional, integral gains of the controller, respectively; x is the controller's state; γ is the controller's fractional order; and u, y, are the control input and unconstrained output, respectively.

3.2 Windup Limiter

The windup limiter model constrains the FOPI output variable y. This model is given by (6) and:

$$w = \begin{cases} w^{\max} & \text{if } y \geq w^{\max} \;, \\ y & \text{if } w^{\min} < y < w^{\max} \;, \\ w^{\min} & \text{if } y \leq w^{\min} \;, \end{cases} \tag{7}$$

where w is the limited output of the controller.

3.3 Anti-windup Limiters

The anti-windup techniques considered are:

- Back calculation: The back calculation method reduces the controller's integral windup through a feedback signal with a gain, when the output is at its limit. This model is given by (7) and:

$$\begin{aligned} x^{(\gamma)} &= u k_i + k_s z \;, \\ y &= k_p u + x \;, \end{aligned} \tag{8}$$

  where $z = w - y$ and k_s, are the feedback signal and gain, respectively.
- Automatic reset: This model considers a saturated input to the forward signal of the controller. Therefore, if the output exceeds its limit, a constrained input reduces the integral action which in turn prevents the windup. This model is given by (7) and:

$$\begin{aligned} x^{(\gamma)} &= \frac{1}{T_i}(w - x) \;, \\ y &= k_p u + x \;, \end{aligned} \tag{9}$$

  where $T_i = \dfrac{k_p}{k_i}$.
- Conditional integrator: The conditional integrator method sets the input of the FOPI integrator block to zero, when the control output is beyond its limits and the control input and output have the same sign, as follows:

$$\begin{aligned} &\text{if } y \geq w^{\max} \;\&\; uy > 0 : w = w^{\max} \;\&\; x^{(\gamma)} = 0 \;, \\ &\text{if } y \leq w^{\min} \;\&\; uy > 0 : w = w^{\min} \;\&\; x^{(\gamma)} = 0 \;, \\ &\qquad\qquad \text{otherwise} : w = y \;\&\; x^{(\gamma)} = k_i u \;. \end{aligned} \tag{10}$$

3.4 Numerical Issues of the Conditional AW model

The conditional AW technique is recommended by the IEEE Standard 421.5-2016 for power system dynamic studies (IEEE, 26 Aug. 2016). Implementation difficulties, as well as numerical issues that emerge during time domain simulations with inclusion of this model for the integer-order PI controller have been adressed (Hiskens, 2012; Murad and Milano, 2019). However, the structure of an ORA-based FOPI controller is different from that of the integer-order PI, and thus, the two implementations do not share the same numerical issues. Here we describe a numerical issue of the conditional AW model that occurs for ORA-based FOPI controllers.

Let us consider a time domain simulation with inclusion of a FOPI with conditional AW limiter. The FOPI input is arbitrary and no limit is binding until $t = t_1$, i.e. the controller is in its integrating region. At $t = t_1$, the control

output reaches its maximum for a positive input value $u(t_1) > 0$. Then from (10):

$$x(t_1) + k_p u(t_1) = w^{\max} \ . \tag{11}$$

For simplicity but without loss of generality, let us consider that the ORA order is $N = 1$. Combining (5) and (11) yields:

$$\begin{aligned} w^{\max} &= \big(\boldsymbol{C}\chi_1(t_1) + \omega_h^{\gamma} u(t_1)\big)k_i + k_p u(t_1) \ , \\ \chi_1'(t_1) &= \boldsymbol{A}\chi_1(t_1) + \boldsymbol{B}u(t_1) \ . \end{aligned} \tag{12}$$

We consider the backward Euler integration method with step size h. Then, $\chi_1(t_1)$ is obtained as:

$$\begin{aligned} \chi_1(t_1) - \chi_1(t_1 - h) = h\chi_1'(t_1) = h\big(\boldsymbol{A}\chi_1(t_1) + \boldsymbol{B}u(t_1)\big) \ , \\ \Rightarrow \chi_1(t_1) = \frac{h\boldsymbol{B}u(t_1) + \chi_1(t_1 - h)}{1 - h\boldsymbol{A}} \ . \end{aligned} \tag{13}$$

The value of the output variable is $y(t_1) = w^{\max} > 0$, and thus we have $y(t_1)u(t_1) > 0$. Correspondingly, the control input switches to 0, according to (10). Re-calculating $\chi_1(t_1)$ for the zero input $u(t_1) = 0$, we get:

$$\begin{aligned} \chi_1(t_1) - \chi_1(t_1 - h) = h\chi_1'(t_1) = h\boldsymbol{A}\chi_1(t_1) \ , \\ \Rightarrow \chi_1(t_1) = \frac{\chi_1(t_1 - h)}{1 - h\boldsymbol{A}} \ . \end{aligned} \tag{14}$$

Observe that $\chi_1(t_1 - h)$ is constant in (13) and (14), while $\boldsymbol{A}, \boldsymbol{B}, h$ are positive. Thus, from (13) to (14), the value of the integrator state variable decreases. This results in a decrease of the output below its maximum value so that (11) is not satisfied anymore. However, at the same time step, the controller starts integrating and the condition for switching back to maximum becomes true again. Finally, a chattering between the maximum and integrating region occurs at t_1 and the solver fails to converge. This chattering problem occurs even if a different implicit integration method is considered.

Note that the solver can be designed to continue the simulation by changing the input only at the next time step. Nevertheless, this strategy also introduces numerical chattering until there is a sufficient decrease of the input and the solution reaches back to the integrating range.

4. CASE STUDY

This section presents the VSC-based STATCOM model and discusses the dynamic response of the examined FOPI control schemes.

4.1 VSC-based STATCOM

The STATCOM is a shunt flexible AC transmission device that regulates the AC voltage through reactive power support at the bus where it is connected. In this work, reactive power from the STATCOM is based on a VSC. The model of the converter of the VSC is an average value model consisting of an AC/DC converter, a DC-side condenser and an AC-side transformer.

The VSC employs a vector-current control based on dq-composition with grid voltage as phase reference (Amirnaser and Reza (2012)). The converter and its control loops are shown in Fig. 4. The d and q components in the outer control loop are utilized to control the DC and AC voltages, respectively, while the inner loop controls

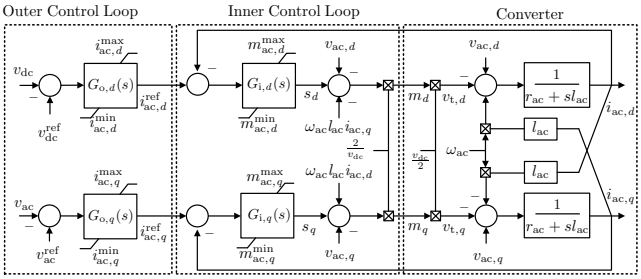

Fig. 4. VSC converter with its inner and outer control in dq-frame.

Table 1. Parameters of VSC-based STATCOM.

Name	**Values**
Converter	$r_{\text{ac}} = 0.001$ pu, $x_{\text{ac}} = 0.05$ pu
Current Limits	$i_{\text{ac},q}^{\text{lim}} = \pm 0.2$ pu, $i_{\text{ac},d}^{\text{lim}} = \pm 0.01$ pu
Outer Control	$k_p^{\text{o},q} = 1$, $k_p^{\text{o},d} = 20$, $k_i^{\text{o},q} = 37.5$, $k_i^{\text{o},d} = 45$, $\gamma^{\text{o},q} = 0.7$, $\gamma^{\text{o},d} = 0.7$, $v_{\text{ac}}^{\text{ref}} = 1.056$, $v_{\text{dc}}^{\text{ref}} = 1$
Inner Control	$k_p^{\text{i},q} = 0.16$, $k_p^{\text{i},d} = 0.16$, $k_i^{\text{i},q} = 0.2$, $k_i^{\text{i},d} = 0.2$, $\gamma^{\text{i},q} = 0.7$, $\gamma^{\text{i},d} = 0.7$

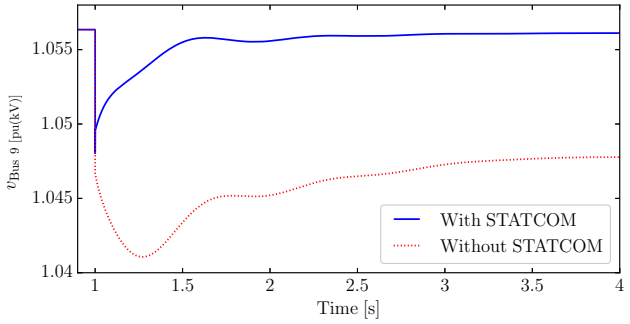

Fig. 5. Response of the voltage at bus 9.

the decoupled d and q currents. In this scheme, $G_{\text{o},d}(s)$, $G_{\text{o},q}(s)$, $G_{\text{i},d}(s)$ and $G_{\text{i},q}(s)$ are FOPI controllers.

4.2 Test System

We consider the IEEE 14-bus system to compare the FOPI models within the VSC control. This system comprises 14 buses, 5 synchronous generators, 11 loads, 12 transmission lines, 4 transformers and 1 shunt capacitor. All the generators are equipped with automatic voltage regulators, and the generators at buses 1 and 2 include turbine governors. The static and dynamic data of this system are given in (Milano (2010)).

A STATCOM is connected at bus 9 for AC voltage control. The data of the STATCOM are given in Table 1. Regarding the FOPIs ORA parameters, the frequency range is set to $[10^{-3}, 10^{2}]$ rad/s and the dynamic order is $N = 5$ for all FOPIs. Unless otherwise stated, the value $k_s = 50$ is used for the back calculation gain of FOPI2. All simulation results are obtained using the Python-based power system software tool DOME (Milano (2013)).

4.3 Contingency I

The performance of the STATCOM voltage regulation is evaluated by increasing the active and reactive power

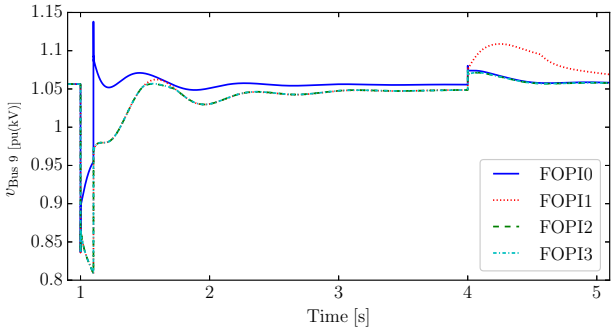

Fig. 6. Response of the voltage at bus 9 considering FOPI0-FOPI3 for the disturbance discussed in Section 4.4.

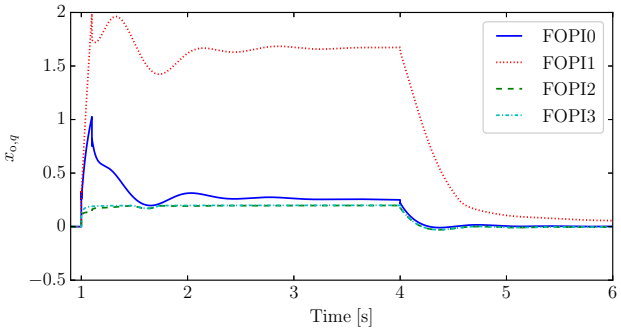

Fig. 7. Response of the integrator state variable of AC voltage controller at outer level.

consumption at buses 3 and 9 by 20% at $t = 1$ s. The voltage response of bus 9 with and without the STATCOM is shown in Fig. 5. The STATCOM provides a fast voltage control without any steady state error. Note that for this disturbance the limits are not binding for any controller in the outer and inner level. Therefore, all FOPIs (FOPI0-FOPI4) provide exactly the same dynamic response.

4.4 Contingency II

For the purpose of comparing the impact of all FOPIs on the system transient response, a severe contingency is considered here. The contingency is a three phase fault that occurs at bus 4 at $t = 1$ s. The fault is cleared after 100 ms through the tripping of the lines that connect buses 4-5 and 4-2. Both lines are back in service at $t = 4$ s. For this disturbance the limits of FOPI1-FOPI4 are activated in the AC voltage controller. Following the contingency, the response of the voltage at bus 9 for the controllers FOPI0-FOPI3 is shown in Fig. 6. Observe that different FOPIs show significantly different transient response. Regarding FOPI4, the simulation with this model cannot be completed due to the numerical issues explained in Section 3.4. To further explain the differences in the voltage response, the fractional integrator state is shown in Fig. 7 for FOPI0-FOPI3.

FOPI0 does not consider any limit and can provide the amount of reactive power that is needed to achieve the reference AC voltage setting. Therefore, the voltage sag during the fault is lower and after clearing the fault the voltage reaches to the pre-disturbance equilibrium. Obviously, the unconstrained model is not realistic for large disturbance analysis.

The models FOPI1-FOPI3 provide a similar response of the voltage until $t = 4$ s (see Fig. 6), since the FOPIs output is always limited at the same value. In addition, for FOPI1-FOPI3, there exists a steady state error until $t = 4$ s and, hence, despite the similar voltage response during the first few seconds, FOPI1 does wind-up (see Fig. 7). Therefore, this model shows a delayed response with a large overshoot when the system finally restores to the pre-disturbance condition at $t = 4$ s. On the other hand, the anti-windup techniques FOPI2-FOPI3 reduce the integrator's input when a limit is binding and thus do not allow the wind-up. This, in turn, provides an overall better transient response.

4.5 Effect of Back Calculation Gain

The back calculation gain (k_s) in FOPI2 determines the speed and level at which the integrator state variable settles when a limit is binding. To show the impact of k_s, the 14-bus system is simulated by applying the same disturbance as in Section 4.4 for different values of k_s. In Fig. 8, the trajectories of the FOPI2 integrator state variable as k_s varies are compared with the one of FOPI3. In order to obtain a faster wind-down of the integrator (see zoom in Fig. 8), a relatively high value of k_s is required. On the other hand, FOPI3 always limits the integrator input at the saturation level and therefore does not provide any flexibility for a faster wind-down.

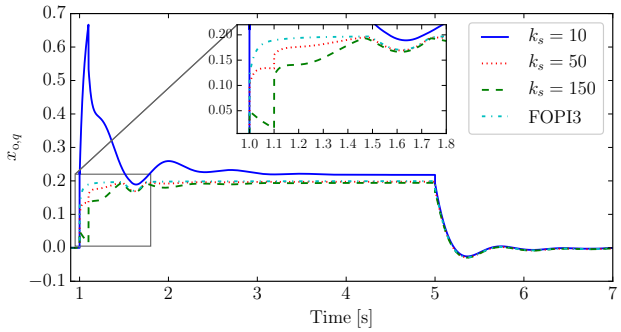

Fig. 8. Response of the integrator state variable of AC voltage controller at outer level for: (i) FOPI2 with different k_s values; (ii) FOPI3.

4.6 Contingency III

To show the dynamic response of FOPI4 when the solver continues through numerical chattering (see Section 3.4), the generator at bus 8 and the shunt device at bus 9 are disconnected at $t = 1$ s and re-connected at $t = 3$ s. Following the contingency the response of bus 9 voltage is shown in Fig. 9 for all the FOPIs. For this disturbance the limits of the AC voltage controller binds in between $1-3$ s for FOPI1-FOPI4. Observe that, in the same time interval, using FOPI4 causes the voltage response to chatter (zoom in Fig. 9) due to the numerical issues discussed in Section 3.4.

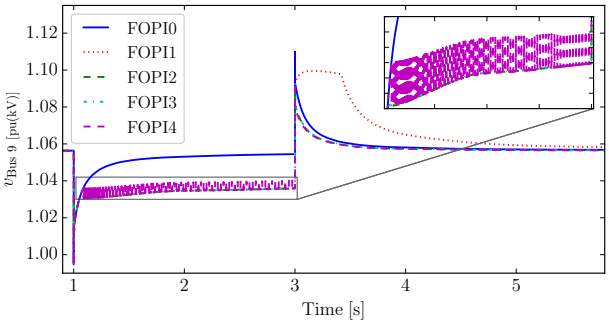

Fig. 9. Response of the voltage at bus 9 considering FOPI0-FOPI4 for the disturbance discussed in Section 4.6.

5. CONCLUSION

This paper presents the windup and anti-windup models of fractional-order PI controllers for a VSC-based STATCOM. The dynamic behaviors of all models are compared and discussed.

Simulation results indicate that, if a FOPI controller-based application is used in a power system software tool for dynamic analysis, the model should consider an appropriate AW method. Among the three most common AW methods, the back calculation (FOPI2) and the automatic reset method (FOPI3) are preferred compared to the conditional integrator method (FOPI4). Moreover, whenever the FOPI2 is employed the back calculation gain should be properly tuned.

Future work will further investigate the numerical issues of the conditional integration anti-windup method and propose suitable solutions.

REFERENCES

Abdulkhader, H.K., Jacob, J., and Mathew, A.T. (2019). Robust type-2 fuzzy fractional order PID controller for dynamic stability enhancement of power system having res based microgrid penetration. *International Journal of Electrical Power & Energy Systems*, 110, 357 – 371.

Amirnaser, Y. and Reza, I. (2012). *Voltage-sourced converters in power systems: modeling, control, and applications*. IEEE Press.

Åström, K.J., Hägglund, T., and Astrom, K.J. (2006). *Advanced PID control*, volume 461. ISA-The Instrumentation, Systems, and Automation Society Research Triangle.

Baranowski, J., Bauer, W., Zagórowska, M., Dziwiński, T., and Piatek, P. (2015). Time-domain oustaloup approximation. In *2015 20th Intern. Conference on Methods and Models in Automation and Robotics (MMAR)*, 116–120.

Bode, H. (1945). *Network Analysis and Feedback Amplifier Design*. Van Nostrand.

Chaib, L., Choucha, A., and Arif, S. (2017). Optimal design and tuning of novel fractional order PID power system stabilizer using a new metaheuristic Bat algorithm. *Ain Shams Engineering Journal*, 8(2), 113 – 125.

Debbarma, S., Saikia, L.C., and Sinha, N. (2014). Automatic generation control using two degree of freedom fractional order PID controller. *International Journal of Electrical Power & Energy Systems*, 58, 120 – 129.

Glattfelder, A.H. and Schaufelberger, W. (2012). *Control systems with input and output constraints*. Springer Science & Business Media.

Hiskens, I.A. (2012). Dynamics of type-3 wind turbine generator models. *IEEE Transactions on Power Systems*, 27(1), 465–474.

IEEE (26 Aug. 2016). IEEE recommended practice for excitation system models for power system stability studies.

Milano, F. (2010). *Power System Modelling and Scripting*. Springer, London.

Milano, F. (2013). A Python-based software tool for power system analysis. In *Proceedings of the IEEE PES General Meeting*. Vancouver, BC.

Monje, C.A., Chen, Y., Vinagre, B.M., Xue, D., and Feliu, V. (2010). *Fractional-order Systems and Controls, Fundamentals and Applications*. Springer.

Murad, M.A.A. and Milano, F. (2019). Modeling and simulation of PI-controllers limiters for the dynamic analysis of VSC-based devices. *IEEE Transactions on Power Systems*, 34(5), 3921–3930.

Oustaloup, A. (1991). *La commande CRONE (commande robuste d'ordre non entier)*. Hermés, Paris.

Oustaloup, A., Levron, F., Mathieu, B., and Nanot, F.M. (2000). Frequency-band complex noninteger differentiator: characterization and synthesis. *IEEE Transactions on Circuits and Systems I: Fundamental Theory and Applications*, 47(1), 25–39.

Padula, F., Visioli, A., and Pagnoni, M. (2012). On the anti-windup schemes for fractional-order PID controllers. In *Proceedings of 2012 IEEE 17th International Conference on Emerging Technologies & Factory Automation (ETFA 2012)*, 1–4. IEEE.

Pan, I. and Das, S. (2015). Fractional-order load-frequency control of interconnected power systems using chaotic multi-objective optimization. *Applied Soft Computing*, 29, 328 – 344.

Pandey, S., Dwivedi, P., and Junghare, A. (2017). A novel 2-DOF fractional-order PI^{λ}-D^{μ} controller with inherent anti-windup capability for a magnetic levitation system. *aeu-international journal of electronics and communications*, 79, 158–171.

Podlubny, I. (1999a). *Fractional differential equations, volume 198: an introduction to fractional derivatives, fractional differential equations, to methods of their solution and some of their applications*. Academic Press.

Podlubny, I. (1999b). Fractional-order systems and $PI^{\lambda}D^{\mu}$-controllers. *IEEE Transactions Automatic Control*, 44(1), 208–214.

Shah, R., Preece, R., and Barnes, M. (2018). The impact of voltage regulation of multiinfeed VSC-HVDC on power system Stability. *IEEE Transactions on Energy Conversion*, 33(4), 1614–1627.

Vinagre, B.M., Podlubny, I., and Feliu, V. (2000). Some approximations of fractional order operators used in control theory and applications. *Fractional calculus and applied analysis*, 231–248.

Zamani, M., Karimi-Ghartemani, M., Sadati, N., and Parniani, M. (2009). Design of a fractional order PID controller for an AVR using particle swarm optimization. *Control Engineering Practice*, 17(12), 1380 – 1387.